Orthogonal Superposition on the ARES-G2

Keywords: Orthogonal superposition, FRT, Orthogonal double wall Couette, anisotropy, structural changes, DMA, tension, compression, bending

RH035

INTRODUCTION

The principle of orthogonal superposition refers to applying a small amplitude oscillation in the transverse direction of a steady shear flow, and dates back to developments of Philippoff (1934)[1], Birnboim and Ferry (1961)[2], Simmons (1966)[3], Zeegers (1995)[4]. In 1997 Jan Vermant et al.[5] implemented orthogonal superposition on steady shear capability on a commercial rheometer (RMS800). The FRT normal force transducer of the RMS800 was modified to perform an axial sinusoidal displacement instead of controlling the transducer shaft at a null position. The double wall geometry (according to Zeegers and Simmons suggestions) was modified to reduce pumping effects during axial displacement of the upper cylinder. In 2009 Mobuchon[6] implemented the same modification on an ARES rheometer to apply an axial oscillation onto a angular oscillating shear (2D – SAOS) to study anisotropy effects in silicate suspensions.

The orthogonal superposition (OSP) feature is now fully integrated into the ARES-G2 and extends the instrument capabilities as follows:

- OSP on steady shear to monitor structural changes under non-linear flow conditions. This method is a possible alternative to LAOS experiments to study non-linear flow effects
- 2D-SAOS to quantify anisotropy in materials
- DMA for tension/compression and bending testing
- Multiaxial testing on soft solids such as gels, foams, etc.

FRT TRANSDUCER

The FRT or force rebalance transducer is a quasi-noncompliant sensor for torque and normal force over a wide dynamic range, used on the ARES rheometer. The quasinoncompliant measurement is accomplished by controlling the transducer shaft to a .fixed position, in both angular and axial directions. The torque and axial force required to hold the motor shaft at the same position are the measured signals. Since the shaft is not moving, instrument inertia contributions to the force and torque measurement are not present[7].

For OSP measurements, the normal force control loop of the FRT transducer has been modified to allow the motor shaft to oscillate at fixed amplitude and frequency. The force required to apply the displacement is measured as before. Since the transducer shaft is moving axially, transducer inertia contributions now need to be corrected for. In this new configuration, the normal transducer operates like a stress controlled (single head) rheometers. As such the

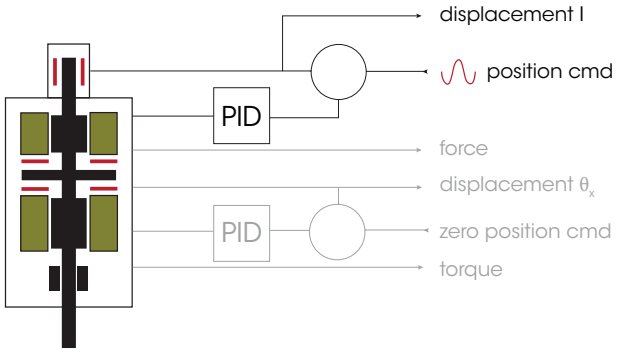

Figure 1: Schematical representation of the normal force transducer/ actuator.

transfer function of the normal force transducer without any sample needs to be determined to obtain the system contributions, necessary to correct the measured force signal. The normal transducer/actuator is modelled using a second order transfer function with an inertia term or mass (m), a drag (friction) term (ζ) and an elasticity (spring) term (K). The measured raw stiffness and raw drag coefficient as a function of the angular frequency are shown in figure 2. At high frequency the raw stiffness has a slope of 2 in the log-log representation and the phase is approaching 180 °. From the slope a system mass of 676g is extracted. In the middle range (10^{-1} to 10 rad/s) the raw stiffness has a slope of 1 with respect to the angular frequency. The raw drag coefficient is frequency independent in this frequency range and the phase approaches 90°. The drag term (9.54 N.s/m) is taken from the drag coefficient curve at the frequency where the phase equals 90 °. At low frequency the raw stiffness approaches a constant value as the measured force reaches a plateau value of ~3 10^{-5}N (30 mg). This is to low end force limitation of the transducer. The raw stiffness plateau (0.53 N/m) provides the elasticity coefficient.

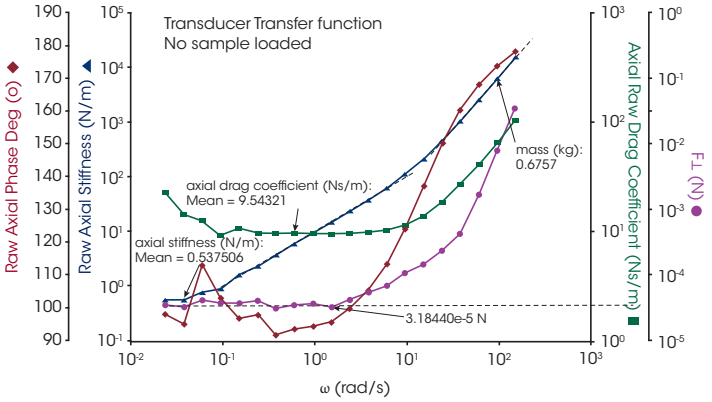

Figure 2. Transfer function of the transducer/actuator without any sample as a function of frequency.

With the three parameters, system mass, drag coefficient and elasticity coefficient the transfer function of the transducer is well characterized and the measured force signal can be corrected for to obtain the sample stress.

In order to prove the performance of the normal actuator/ transducer, a frequency sweep was performed on the TAI internal PIB standard PIB 1490 and the dynamic moduli were measured in both angular (traditional measurement) and in axial (using the normal force transducer) direction.

Good agreement is obtained over the frequency range from 0.1 to 100 rad/s (figure 3). A slight deviation at 100 rad/s is observed in the phase angle; there is some phase shift in addition to the inertia phase correction, which is not compensated for. At low frequency G` and the phase in the proximity of 90 ° becomes noisy. The measured force is close to the low end limit of the normal force transducer in this case.

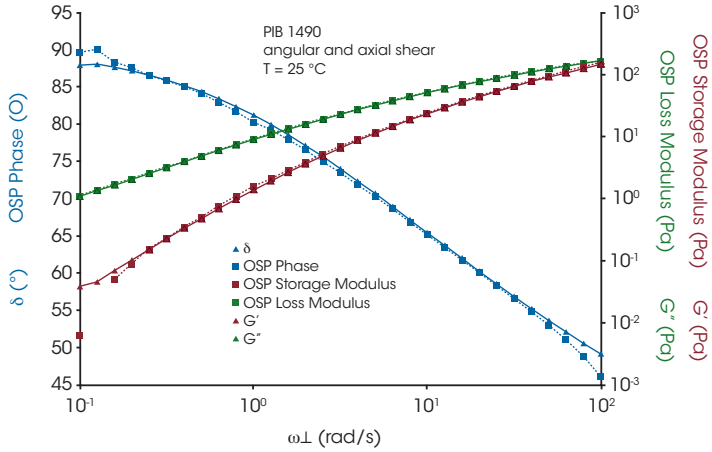

Figure 3: Frequency response of a PIB (PIB 1490 internal reference) sample measured in rotation (standard) and axial (OSP) direction on the ARES-G2.

OSP GEOMETRY

Early OSP measurements by Simmons[3] have been performed with standard concentric cylinder system. Zeegers[4] used a double wall concentric cylinder geometry. The OSP used in the following is a double wall concentric cylinder system, modified to eliminate/ reduce boundary effects according to suggestions of Simmons[3]. The double wall concentric system for orthogonal superposition (Figure 4) consists of 3 parts:

- the inner cylinder attached to the motor,
- the center cylinder attched to the transducer and
- the outer cylinder, attached to the inner cylinder base.

The outer cyinder can be removed for easy cleaning. The wall thickness of the center cylinder determines the gap size. Two center cylinders for a nominal 1mm and 0.5mm gap are available. The inner and outer gap have different size because they are designed to provide the same average angular shear rate. The axial shear rate is based on the gap average.

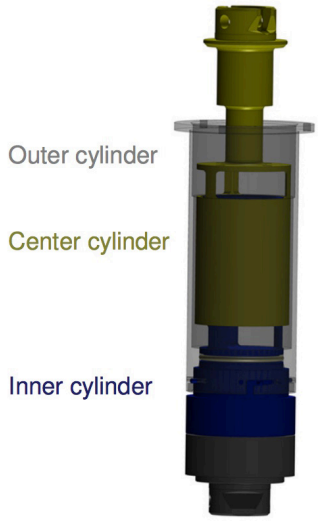

Figure 4: OSP double wall concentric cylinder system with upper and lower windows, assembled.

The inner cylinder (blue) as well as the center cylinder (dark yellow) have 3 windows either at the bottom or the top (Figure 5). The center cylinder section is aligned with the inner cylinder such that the shear surfaces above and below the windows overlay. The nominal shear surface is the distance between the windows at the top and the bottom of the center and inner cylinder.

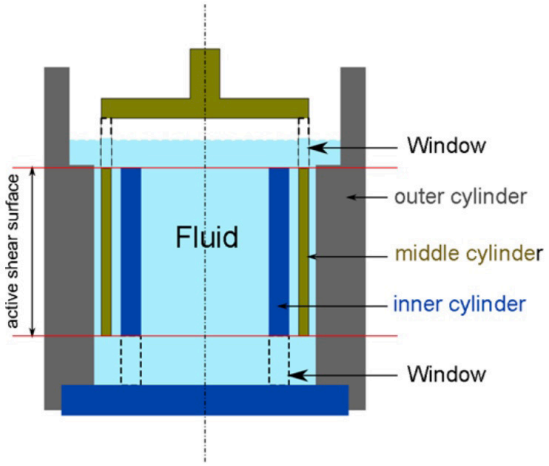

Figure 5: Schematical representation of the OSP flow cell. Windows at the top and bottom allow free circulation of the fluid when the center cylinder is displaced vertically. This reduces pumping effects at the bottom of the cell and surface tension effects at the top.

The windows at the bottom of the inner cylinder and the windows at the top of the center cylinder allow the fluid to communicate between the inner, outer gap and the hollow inner cylinder.

The windows at the bottom of the inner cylinder allow for the fluid to evacuate into the hollow inner cylinder reservoir thus reducing the backflow of the fluid in the gap (pumping effect). However the evacuation flow does not remain unnoticed and increases the measured force at the center cylinder. The boundary effects at the bottom of the cup can

be minimized to approximately 10% of the measured force and are compensated for by a front factor in the geometry constant.

The windows at the top of the center cylinder guarantee that the fluid level remains the same in the two gaps and the reservoir at all times. This design eliminates surface tension effects which otherwise would increase the measured force. Due to the vertical displacement, work would had to be done against the surface tension because of the changing fluid-air interface area (Figure 6).

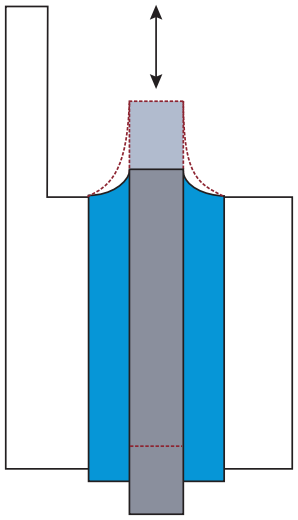

Figure 6: Effect of surface tension during the vertical motion of the center cylinder in the windowless design. An increase of the surface area would generate an additional force contribution due to work done against the surface tension at the air-fluid interface.

Without upper windows in the center cylinder, interfacial tension can significantly alter the test results as shown in Figure 7. Surface tension contributions alter the elastic axial stiffness. With an empty geometry (no sample loaded), the low frequency axial stiffness is 14.8 N/m for the given test setup. When silicone oil is loaded, the elastic stiffness increases to 21.3 N/m and with water increases even further to 27.4 N/m. Since the surface tension is a purely elastic contribution, the measured phase approaches 0 ° when surface tension dominates the response at low frequency.

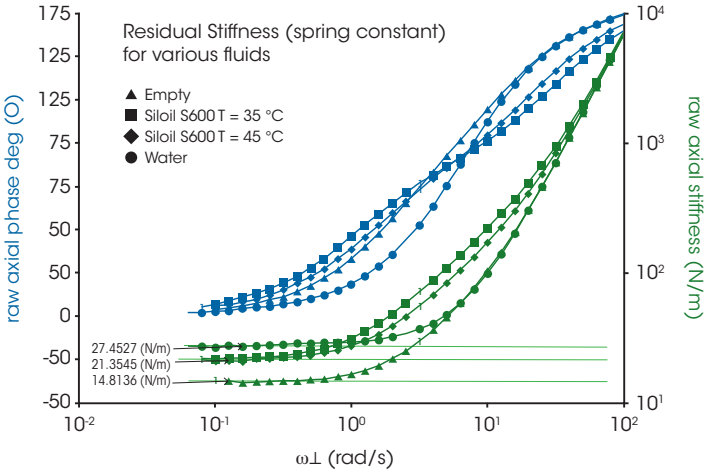

Figure 7: Effect of surface tension of various fluids on the axial spring constant of the transfer function.

The surface tensioncontribution is a not negligible and a sample dependent correction of the elasticity coefficient would be required. By adding the upper windows, the interfacial surface effects can be eliminated. The elastic system coefficient K in this case is sample independent and in the final design has a value, typical around 1N/m. This is in the range of the sensitivity of the normal force transducer.

The geometry constants for stress and strain in axial direction are based on the derivations by Markowitz in 1952[8]. In the equations the fluids inertia correction is omitted. The current force sensitivity of the transducer does not allow measurement of fluids with a viscosity low enough for the fluids inertia contributions to be significant in the double wall concentric cylinder system.

The details for the two OSP geometries with 0.5 and 1.0 mm nominal gap are shown in table 1. Note also that because of the high axial stiffness of the geometry, no axial compliance correction is necessary.

Geometry:	1.0mm nominal gap		0.5mm nominal gap	
Volume:	37mL		32.7 mL	
Mass:	72.61g		93.245g	
Inertia:	10.3 μNms²		15.5 μNms²	
	Rotation	Axial	Rotation	Axial
K_g =	17.16 [1/rad]	1080.42 [1/m]	33.81 [1/rad]	2117.90 [1/m]
K_s =	6524.05 [Pa/Nm]	100.46 [Pa/N]	7511.93 [Pa/Nm]	116.26 [Pa/N]

Table 1: Axial and angular geometry constants for the 0.5 and 1mm OSP geometries.

EXPERIMENTAL RESULTS ON PIB 1490 & HPC

Effect Of Steady Shear On Superposed Orthogonal SAOS

The changes of the viscoelastic response of a PIB solution in decane during flow were monitored in orthogonal oscillatory shear, superimposed onto a steady shear at shear rates from 0 to 5 1/s. The material was probed at an orthogonal shear strain of 2% in a frequency range from 0.1 to 100 rad/s. The cross over point frequency for this material at room temperature is higher than 100 rad/s - thus outside of the operation range of the normal force transducer in OPS mode.

Figure 8 exhibits the viscoelastic behavior of the PIB solution at rest in both, axial and angular directions. The results obtained in the two shearing directions virtually superpose. It should be noted that the uncorrected values obtained in axial shear are about 13% higher than those obtained in rotational shear. A front factor implemented in the geometry stress constant corrects for this geometry effect. The slight deviation of G' at a frequency of 0.1 rad/s can be attributed to the lower sensitivity of the normal force sensor in relation to the torque sensor.

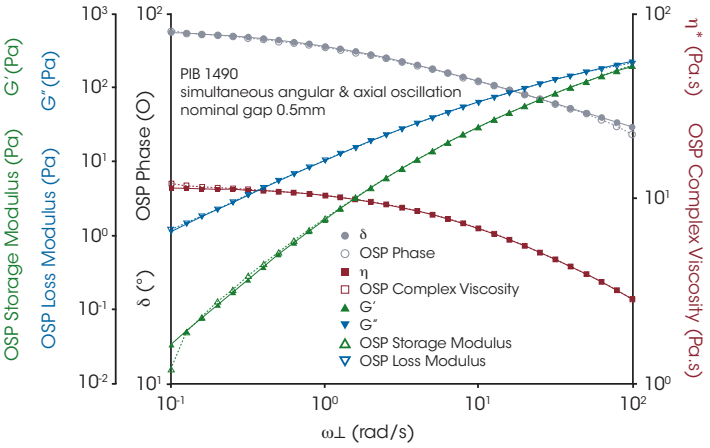

Figure 8: Viscoelastic response for the internal PIB reference solution PIB1490 in angular and axial shear at a strain of 2%.

In figure 9 the viscoelastic response is shown when an orthogonal steady shear applied in the range from 0.01 to 5 1/s. As the steady shear is increased, the storage and loss moduli decrease in the terminal region, the PIB1490 behaves more and more viscous and the phase (not shown in figure 9) shift towards 90 °. The complex viscosity in the terminal region drops by an order of magnitude while the shear rate increases by an order of 2.5.

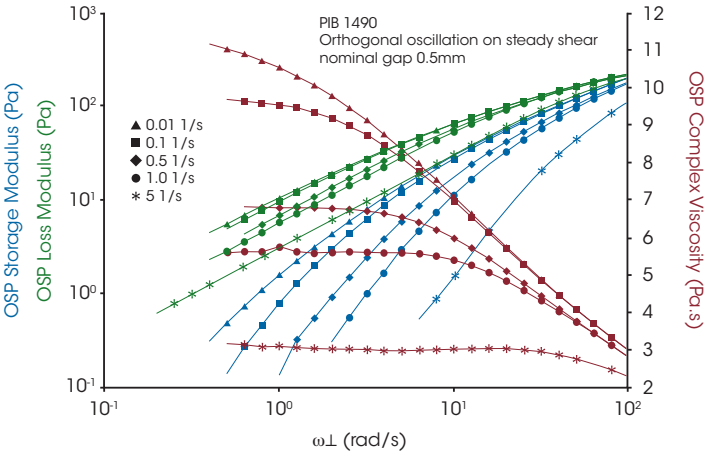

Figure 9: Viscoelastic response for the internal PIB reference solution PIB1490 in axial shear at a strain of 2%, superimposed on a steady shear in a range from 0.001 to 5 1/s.

2D Flow Experiments

In 2D-SAOS experiments, the viscoelastic properties can be measured in all directions within the θ-z plane. A bidirectional flow field is imposed by coupling the axial and angular oscillatory deformations γ_z and γ_θ at a frequency ω and a phase difference δγ between angular strain and linear strain (figure 10) according to:

$\gamma_r = 0$

$\gamma_\theta = \gamma_\theta^\circ \sin(\omega t)$

$\gamma_z = \gamma_z^\circ \sin(\omega t + \delta_\gamma)$

$$G'_{2D} = \frac{\sigma'_{2D}}{\gamma^\circ_{2D}}$$

$$G''_{2D} = \frac{\sigma''_{2D}}{\gamma^\circ_{2D}}$$

$$\delta_{2D} = \tan^{-1}\frac{G''_{2D}}{G'_{2D}}$$

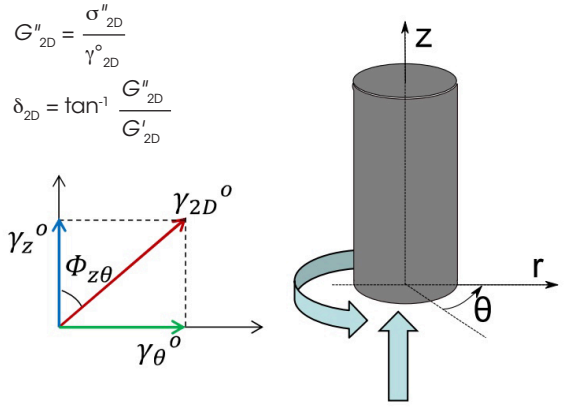

Figure 10: 2D-SAOS measurement using the OSP flow cell.

The measured stress response of the material is:

$\sigma_r = 0$

$\sigma_\theta = \sigma_\theta^\circ \sin(\omega t + \delta_\theta)$

$\sigma_z = \sigma_z^\circ \sin(\omega t + \delta_z)$

Unidirectional flow is maintained when δ_γ is zero; the orientation in repect to the axial direction depends on the ratio of γ_θ/γ_z[6].

$$\gamma^\circ_{2D} = \sqrt{\gamma_\theta^{\circ 2} + \gamma_z^{\circ 2}}$$

$$\phi_{z\theta} = \tan^{-1}\left(\frac{\gamma_\theta}{\gamma_z}\right)$$

The elastic and viscous stress components are calculated as:

$$\sigma'_{2D} = \sqrt{\sigma_\theta'^2 + \sigma_z'^2}$$
$$= \sqrt{\sigma_\theta^{\circ 2}\sin^2\delta_\theta + \sigma_z^{\circ 2}\sin^2\delta_z}$$

$$\sigma''_{2D} = \sqrt{\sigma_\theta''^2 + \sigma_z''^2}$$
$$= \sqrt{\sigma_\theta^{\circ 2}\cos^2\delta_\theta + \sigma_z^{\circ 2}\cos^2\delta_z}$$

The viscoelastic parameters such as the storage and loss moduli are obtained from the components of stress and strain in axial and angular direction.

Figure 11 shows the viscoelastic response of an 8% wt HPC aqueous solution obtained using the 1mm gap OSP double wall concentric cylinder system. HPC (HydroxyPropylCellulose)[9] is a polymer with alternating hydrophobic and hydrophilic groups along the main chain. HPC has a lower critical solution temperature LCST at 45 °C. Below this temperature HPC is readily soluble in water, above this temperature HPC is not soluble. At high concentrations >50%, HPC forms liquid crystals with many mesophases according to its concentration in water.

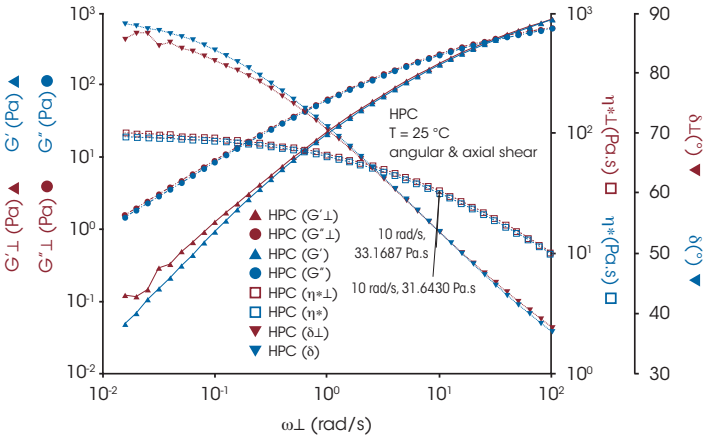

Figure 11: Viscoelastic response of an 8 wt% aqueous HPC solution in angular and axial shear at a strain of 2%.

At room temperature the HPC sample behaves viscoelastic with a pronounced terminal region and a cross over frequency at ~30 rad/s. The zero shear viscosity on the order of 100 Pa.s. Results from tests in angular and axial direction provide almost the same results. Deviations in G' and phase angle can be observed at low frequency due to the force sensitivity limitation of the transducer.

Figure 12 exhibits the axial dynamic moduli G'⊥ and G"⊥ versus frequency at various temperatures when no angular strain excitation is applied. Below 45 °C HPC is soluble in water. At 20, 30 and 40 °C, the material behaves fluid like and the dynamic moduli and the complex viscosity are strongly temperature dependent. Above 45 °C HPC falls out and the HPC solution abruptly changes to gel/solid like behavior with an almost constant phase angle of 20 ° over the measured frequency range (Figure 12a).

Above 50 °C, the mechanical behavior changes very little with temperature and the phase angle is independent of frequency. This is the typical gel like response. Figure 12 b) shows the results replotted for two frequencies 0.1 and 1 Hz as a function of temperature. The LCST transition seperates the mechanical behaviour in a distinct liquid-like and gel-like response.

With axial and angular strain and an offset in phase by $\delta_\gamma = \pi/2$, the deformation becomes two dimensional[6] scanning circularly the shear plane (figure 13). Since the resulting deformation enables to scan the entire shear plane in a single period, it is more suitable to look at a Lissjous plot of the transient angular and axial stress data. As long as the sample is isotropic, the stress response in angular and axial direction is the same and the Lissajous plot is also a circle. When the material behaves anisotropic, the Lissajous becomes an ellipsoid.

With this in mind, temperature sweeps were performed on the HPC sample in 2D oscillation, combining correlation and transient data acquisition. In a first experiment, the temperature was ramped up and down, measuring the dynamic moduli in axial and angular direction in correlation mode (Figure 14). In the liquid like region below LCST, no

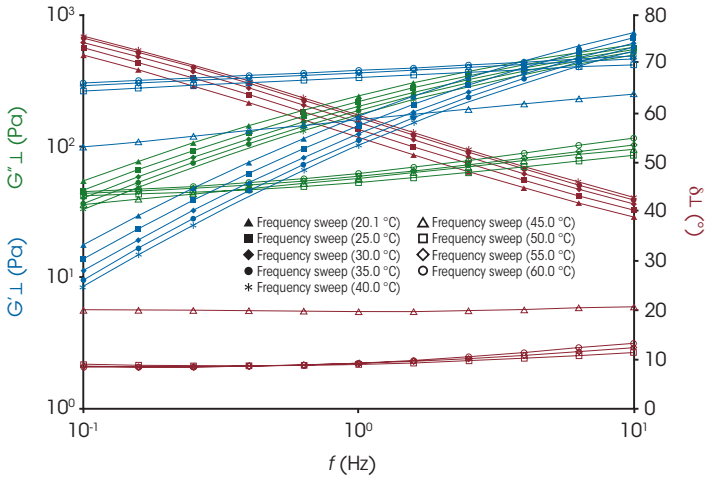

Figure 12 a: Frequency sweep of the HPC 8wt% aqueous solution at various temperatures.

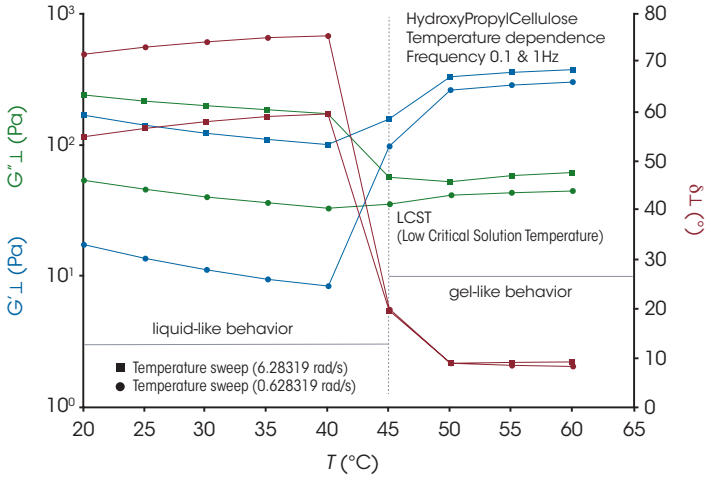

Figure 12 b: Temperature sweep of the HPC 8wt% aqueous solution at a constant frequency of 0.1 and 1 Hz. The LCST transitions separates the liquid-like and the gel-like response.

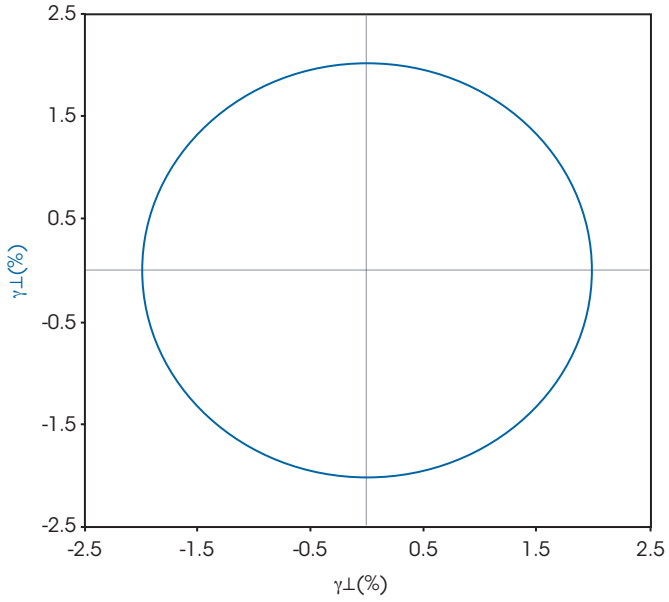

Figure 13: Lissajous plot of axial versus angular transient shear deformation with a phase offset of π/2.

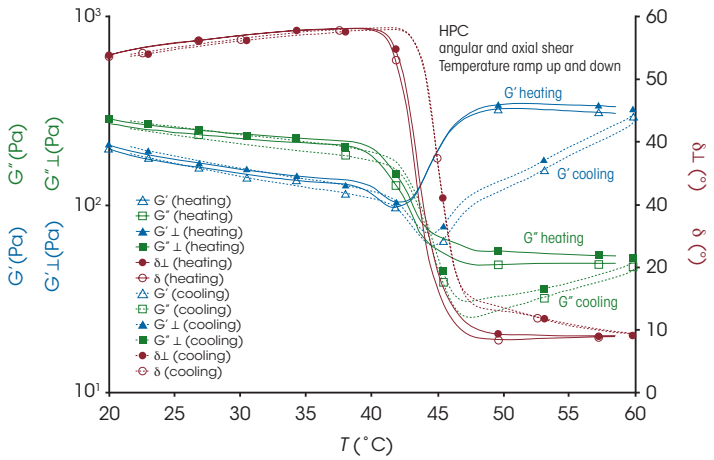

Figure 14: Temperature sweep of the 8 wt% HPC aqueous solution at a constant frequency of 1 Hz. At the LCST, the HPC changes from liquid-like to gel-like behavior. When ramping the temperature from 60 °C down, the viscoelastic response above LCST is very different from the the behavior during heating. Below the transition the moduli G' and G" for the up and down ramp approach each other again.

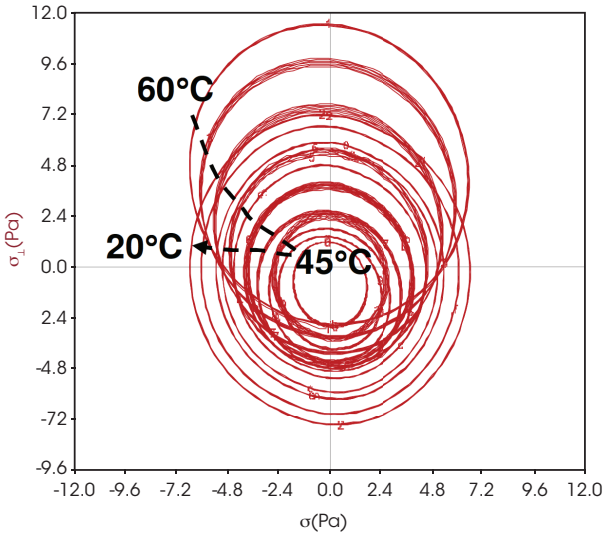

Figure 15: Lissajous plot of the axial versus angular stress response during the cooling from 60 to 25 °C. Note that the axial stress has been offset during the heating.

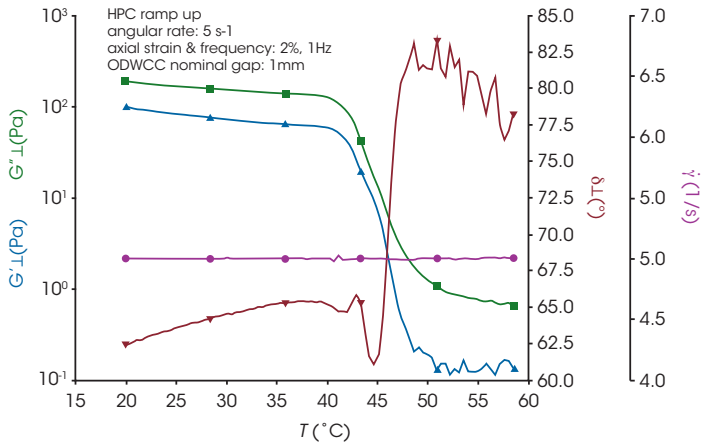

Figure 16a:Temperature sweep of the 8wt% HPC aqueous solution at a constant rate of 5 1/s in angular direction. The material behaviour is monitored at a frequency of 1 Hz in axial direction. At the LCST, both moduli in axial direction drop significantly and the sample remains predominately viscous up to 60 °C.

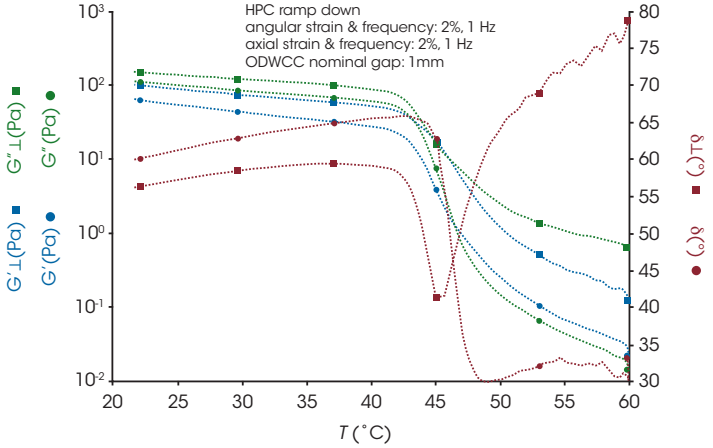

Figure 16b: The cooling ramp monitored with SAOS in angular and axial direction. Note that the behavior in angular direction at high temperature is more elastic - which means that the the shearing during heating through the transition has intoduced significant anisotropy .

difference in G' and G" is found between axial and angular shear. At the critical solution temperature, G" drops almost one order of magnitude while G', after an initial drop increases to a higher equilibrium value in the gel like region. The slight differences in the moduli between axial and angular direction increase marginally above the LCST. During cooling from 60 °C down to 20 °C, G' and G" however follow a different path compared to the heating phase. Both dynamic moduli start decreasing from 60 °C on. At the transition, which occurs at a slighly higher temperature, G" and G' recover; G' goes through a small minimum first. Below the LCST, G' and G" are approaching the heating curve. The structure rearrangements at the LCST during heating introduce only minor anisotropy, which disappears slowly once the sample temperature is below 45 °C.

The test was repeated, however during the cooling phase the transient stress in axial and angular direction was monitored with a phase offset of $\pi/2$ in the input strain components. The results are represented in a Lissajous plot in figure 15. At all temperatures the stress response exhibits almost circular behavior, which means that the material remains isotropic during the the complete cooling cycle. The total stress decreases in the temperature range from 60° to 45°, as expected from figure 14 and then increases again as the temperature increases to 20 °C. However an offset in the axial transducer force has been introduced during the heating cycle; this offset slowly disappearing as the sample is cooled down to 45 °C. It is not quite understood why this offset showed only in axial direction. Note that this offset is rejected by the correlation and as such does not effect the dynamic moduli in figure 14. In a second experiment, the sample was sheared at a constant rate of 5 1/s in angular direction while ramping the temperature up from 20° to 60 °C (figure 16a). Only the dynamic moduli in axial direction were monitored during this experiment. The phase angle increases sharply above 45 °C and both the axial storage modulus and the loss modulus drop significantly. The transition is quite interesting as the phase angle goes through a minimum first and then increases to 80 °; it appears that gel structure starts to build in axial direction at 45 °C followed by structure breakdown due to the imposed shear.

At 60 °C the rotational steady shear is stopped and the cooling behavior is monitored with small amplitude oscillation in angular and axial direction (figure 16b). The first observation to be made is, that at 60 °C the phase angle in angular direction (direction in which the steady shear has been applied) is around 30°, while the phase angle for the orthogonal shear is at 80° (which is consistant with the results from the heating ramp). An explanation is that due to the imposed shear, a weak structure oriented in the direction of the imposed shear builds during the LCST transition. In the orthogonal direction the sample behavior is mostly viscous and dominates the overall response because the complex modulus G⊥* is 1 decade higher than G*. As the temperature decreases, the phase angle in axial direction drops sharply at the LCST transition and goes through a minimum at 45° C . The phase angle in angular direction increases from 30° to 65° at the LCST transition rather quickly. Below the LCST transition the phases in angular and axial direction converge and the sample slowly approaches isotropy.

The cooling process was also monitored using the 2D Lissajous plot of the transient angular and axial stress resulting from the imposed small amplitude strain components, offset by 90°. Above 45° C, the Lissajous is elongated in the normal direction as a result of the higher complex modulus in axial direction (anisotropy). Below 45° C, the Lissajous traces are slowly approaching a circle, indicating that the modulus in angular and axial direction are converging and the sample approaching isotropy as time goes on.

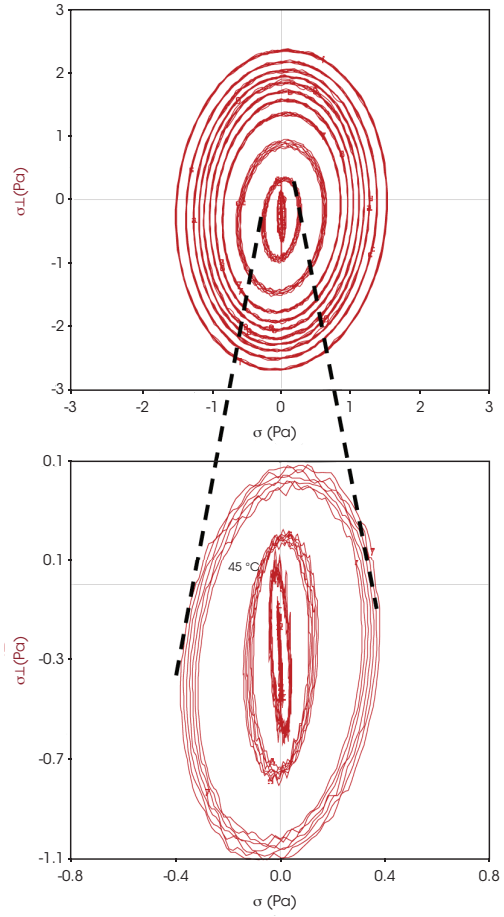

Figure 17: Lissajous plot of the axial versus angular stress response during the cooling from 60 to 25 °C. Notice that the axial stress is much higher than the angular stress.

At 60° C the total stress in axial direction is mostly viscous and much higher than the predominately elastic stress in angular direction. It can be postulated, that the unsoluble HPC is oriented in angular direction, while the development of an overall 3-D structure is prevented by the imposed shear during and above the LCST.

DMA MEASUREMENTS

The new axial oscillatory test capability permits the ARES-G2 to perform linear testing, previously only available on specialized instruments such as the RSA. With this ability, DMA measurements can now be easily performed on the ARES-G2 also.

For DMA measurements, only the normal force transducer is used. The transducer in this case operates like the Q800, with the deformation being imposed and the force measured by the same device. The bottom angular actuator is locked in position during DMA testing. The torque transducer remains active, but is switched to high range to avoid accidental overload.

The test fixtures that can be used are plates (compression), film-fiber clamp (tension) and free and clamped bending geometry.

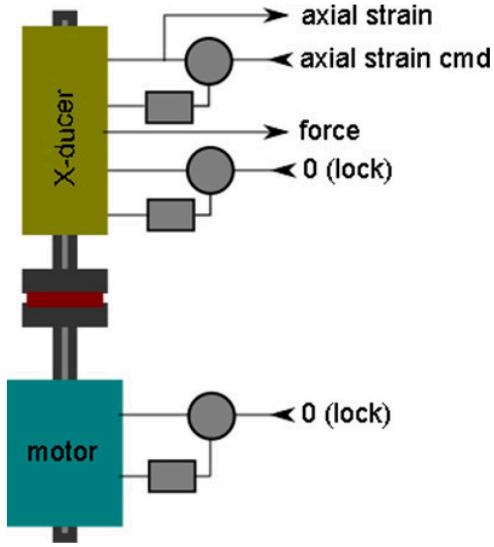

Figure 18: Block diagram of the ARES-G2 in DMA mode.

Figure 19 shows results from temperature sweeps performed on standard ABS and PMMA specimen in the temperature range from 50° C up beyond the glass transition using the tree point bending geometry. The results showed to be almost identical with those obtained on the RSA.

A 50 micron PET film was tested in tension from 50° C up to 250° C (figure 20). The glass transition shows at a temperature of 109° C, the melting point is at 250°. At the melting point the moduli and the phase drop catastrophically.

It should be noted that as the sample was heated, the sample was shrinking due to frozen in orientations. The sample length did only slightly increase below the first peak below 80° C,

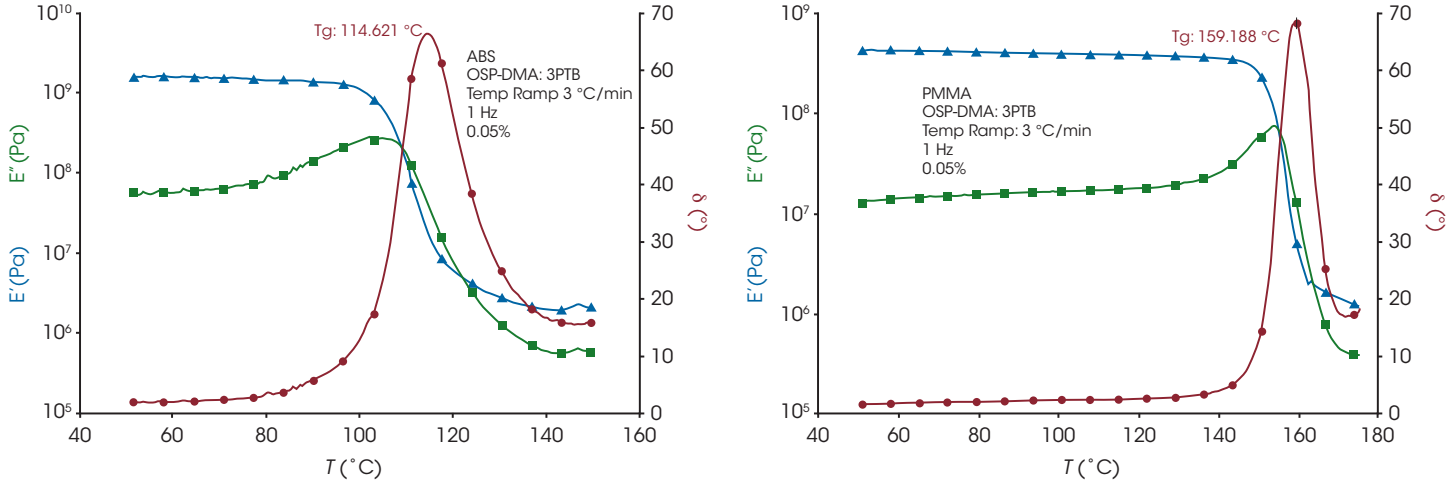

Figure 19: Temperature ramp in three point bending on a) standard ABS, and b)PMMA.

due to material thermal expansion. Since the static force was reduced as the dynamic force decreased with increasing temperature, the internal forces dominated during most of the time and the sample did shrink significantly, almost up to the melting point.

CONCLUSIONS

- A rotational rheometer has been modified to apply an axial (orthogonal) in addition to angular oscillation/transient mode simultaneously (OSP)
- A standard double wall concentric cylinder geometry has been modified to allow a fluid sample to be sheared simultaneously in two orthogonal directions
- Orthogonal superposition at SAOS shear on a steady shear flow to follow structural changes of a material as a function of the flow can be performed
- Superposition of two orthogonal oscillatory shear deformations can be performed to study anisotropy in fluid material samples
- DMA measurements on thin film (tension) and rectangular bars in free and clamped bending can be performed with the same accuracy than standalone DMA's.

ACKNOWLEDGEMENT

This note was written by Aly Franck, TA Instruments.

For more information or to place an order, go to http://www.tainstruments.com/ to locate your local sales office information.

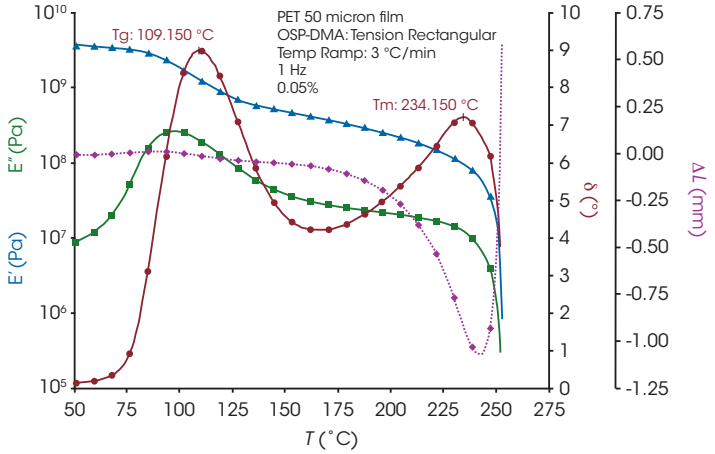

Figure 20: Temperature ramp on a PET film in tension using the film-fibre geometry.

REFERENCES

1. Philiphoff, W., Phys. Z., 35, 884 (1934)
2. BirnBoim M.H., J.D. Ferry, J. Appl. Phys., 32, 2305 (1961)
3. Simmons J.M., J. Sci. Instrum., 43 ,887, (1966)
4. Zeegers J. , D van den Ende, C. Blom, E.G. Altena, G.J. Beukema, J. Mellema, Rheol. Acta 34, 606 (1995)
5. Vermant, J., P.Moldenaers, J.Mewis, M.Ellis, R.Garritano, Rev. Sci. Instrum. 68,4090 (1997)
6. Mobuchon, C., P.J. Carreau, M.-C. Heuzey, J.Rheol. 53, 517 (2009)
7. APN008 FRT technology; Product note TA Instruments
8. Markowitz H., J.appl. Phys. 12:16 1070 (1952)
9. en.wikipedia.org/wiki/Hydroxypropyl_cellulose October 30, 2013.